Phys Chem Minerals (1988) 16:250–261

PHYSICS AND CHEMISTRY OF MINERALS

Defects and Hydrolytic Weakening in α-Berlinite $AlPO_4$ A Structural Analog of Quartz

Bruno Boulogne, Patrick Cordier and Jean-Claude Doukhan
Laboratoire de Structure et Propriétés de l'Etat Solide (associated to C.N.R.S. n° 234),
Université de Lille-Flandres-Artois, 59655 Villeneuve d'Ascq Cedex, France

Abstract. Berlinite, $AlPO_4$, is a structural analog of quartz and a number of physical properties are very similar in both materials. It is thus interesting to compare their mechanical properties and investigate the possible role of water. Constant strain rate tests on wet synthetic crystals have been performed at room temperature and at 600 MPa confining pressure. They indicate that $(0001)1/3\langle 11\bar{2}0\rangle$ is the easy glide system. Detailled investigation of the crystal structure shows that the corresponding **a** dislocations can glide in such a way that only the weaker Al−O bonds are broken. This explains why this glide system is much more easily activated in berlinite than in quartz. Deformation experiments at higher temperature and at atmospheric pressure clearly show a thermally activated regime. However the actually available crystals are so rich in water that above 300° C the dislocation structure resulting from deformation is completely hidden by water precipitation and coarsening of the as-grown fluid inclusions. Like for wet quartz this later phenomenon generates numerous bubbles and sessile dislocation loops.

Introduction

The name berlinite comes from N.J. Berlin who discovered this mineral in Sweden (Palache et al. 1970). In fact this mineral is very rare and the study presented below has been performed on synthetic material. Its interest stems from the fact that berlinite is a structural analog of quartz and a number of physical properties are very similar in both minerals. Like α-quartz, α-berlinite is strongly piezoelectric and potential industrial applications for resonator devices have been considered (see a recent review in Halliburton and Martin 1985; also Detaint et al. 1985). This is the reason why several laboratories have tried to synthesize large and pure single crystals of α-$AlPO_4$ by hydrothermal growth (growth techniques described in Stanley 1954, Kolb and Laudise 1978, Jumas et al. 1987, Chai and Hou 1987). Like for α-quartz grown years ago, this hydrothermal process leads to wet crystals and we show in this study that this water intake influences the mechanical properties of α-berlinite, i.e. a hydrolytic weakening phenomenon occurs. Its mechanism is probably very similar to the one occurring in wet quartz and it has appeared interesting to compare both minerals from this point of view.

In the first section, the defects associated with water are investigated by infrared spectroscopy. The second section is devoted to theoretical considerations on extended lattice defects (dislocations, twins ...). In the third section we report experimental results on plastic deformation tests and associated investigations in *transmission electron microscopy* (TEM) of the resulting dislocation configurations. The role of water and a comparison with the case of quartz are presented in the last section.

Defects Associated with Water

It is weell known that small amounts of water in minerals can be detected by infrared absorption in the wave number range 4000–2500 cm^{-1} which corresponds to the absorption of OH stretching vibrations. Molecular water in tiny fluid inclusions gives rise to a broad absorption band while hydroxyls with precise allocation in the crystal structure lead instead to polarised sharp absorption peaks (Aines and Rossman 1984). The exact position of these peaks in the spectral range of interest depends upon the environment of the vibrating OH's and this has allowed H compensated impurities in quartz to be indirectly characterized (Wood 1960, Kats and Haven 1960, Kats 1962, Dodd and Fraser 1965). This is typically the case of Al substitutional impurities (Lipson and Kahane 1984, 1985). Water has been detected by infrared absorption in a number of minerals (see for instance Freund and Oberheuser 1986 for olivine; Beran 1986 for alkali feldspars; Boland and Tullis 1986 for clinopyroxenes). Quantitative estimates of the H/Si ratio in wet quartz have been evaluated by a number of authors (reviewed in Paterson 1982). In most cases the absorbance spectrum of wet quartz is compared to one of a dry standard and the H/Si ratio is deduced from the measurement of the area bounded by the two spectrum curves. Crystal growers who produce synthetic quartzes for piezoelectric applications estimate the electronic quality factor Q from the absorption ratio of two distinct wave numbers (3500 cm^{-1} where the OH's are active and 3800 cm^{-1} where they do not absorb infrared light). This later method has been transposed to the case of wet berlinite by Steinberg et al. (1984) who propose the following empirical formula for the weight ratio $H_2O/AlPO_4$

$$C(H_2O)=\frac{[H_2O]}{[AlPO_4]}\,(\text{weight ppm})\approx\frac{50}{t}\,\mathrm{Log}_{10}\frac{T_{3800}}{T_{3500}} \qquad (1)$$

where T_x is the intensity of the transmitted light at the considered wave number x and t is the thickness in cm of the sample (basal slab). The former method is less easily

transposed to the case of berlinite because there is no available standard of dry berlinite. This method should however be preferred because the whole spectrum in the range 4000–2500 cm^{-1} contains more information than only two absorption data. In addition, sharp peaks associated with chemical impurities could eventually be detected. We have assumed that water or OH in berlinite, whatever its mode of incorporation, has the same absorption efficiency as in quartz. We have also assumed that the intrinsic absorption of the lattice vibration modes of dry berlinite is negligible. This allows a crude estimate of the water content of wet berlinite crystals to be deduced from the area under the absorption spectrum using a formula commonly used for basal quartz samples

$$C(H_2O)=\frac{[H]}{[Al+P]}(\text{atomic ppm})\approx\frac{1}{t}\int_{4000}^{2500}\text{Log}_{10}\frac{I_\nu}{I_0}d\nu \quad (2)$$

t is the sample thickness in cm, I_ν and I_0 are the transmitted and the incident intensities respectively at the wave number ν (in cm^{-1}). For comparison with formula (1) this atomic concentration can be converted into the weight concentration in H_2O multiplying it by the factor 7.38×10^{-2} (which is the mass ratio $1/2H_2O/AlPO_4=1/2\times18/122$).

Comparison of both methods on a number of crystals grown in various conditions shows that relation (2) leads to water contents 1.2 to 2 times larger than the ones given by relation (1). We have reported in Fig. 1 some typical absorbance spectra. The characteristics of the corresponding samples are given in Table 1. These results suggest several comments:

i) In general berlinite crystals are wet; the driest ones are probably one to two orders of magnitude wetter than high quality synthetic quartz.

ii) There is clearly a broad absorption band in most of these samples extending from approximately 3700 to 2600 cm^{-1}. Whatever the method used to estimate the water content, one notes a general trend of lower water content for higher growth temperatures. This suggests that dry berlinite may be grown at still higher temperatures. In contrast with the case of quartz the solubility of berlinite in most solvants is either extremely small or decreases as T increases (at least at moderate temperature up to 400° C). Consequently the nutrient concentration decreases as well as the growth rate. It is not known if this observed lowering of the water content with increasing growth temperature is to be related to a decrease of the growth rate only or if the solubility of water in berlinite also changes dramatically with the growth conditions (temperature, nutrient concentration ...). The possible influence of pressure is unknown.

iii) In crystals with low to moderate water contents sharps peaks are sometimes superimposed on the broad absorption band. We assume that, in strong analogy with the case of quartz, they are caused by the presence of H compensated impurities. Chemical analyses by mass spectrometry have shown that some samples contain Si and Fe as main impurities (up to 80 at. ppm for Si in one crystal). H compensated $(Si)_P$ and $(Fe^{2+})_{Al}$ could thus account for these peaks. However, up to now, there is no unambiguous correlation between each peak and a given chemical impurity.

It has been assumed for a long time that water enters wet quartz in the form of a supersaturated concentration

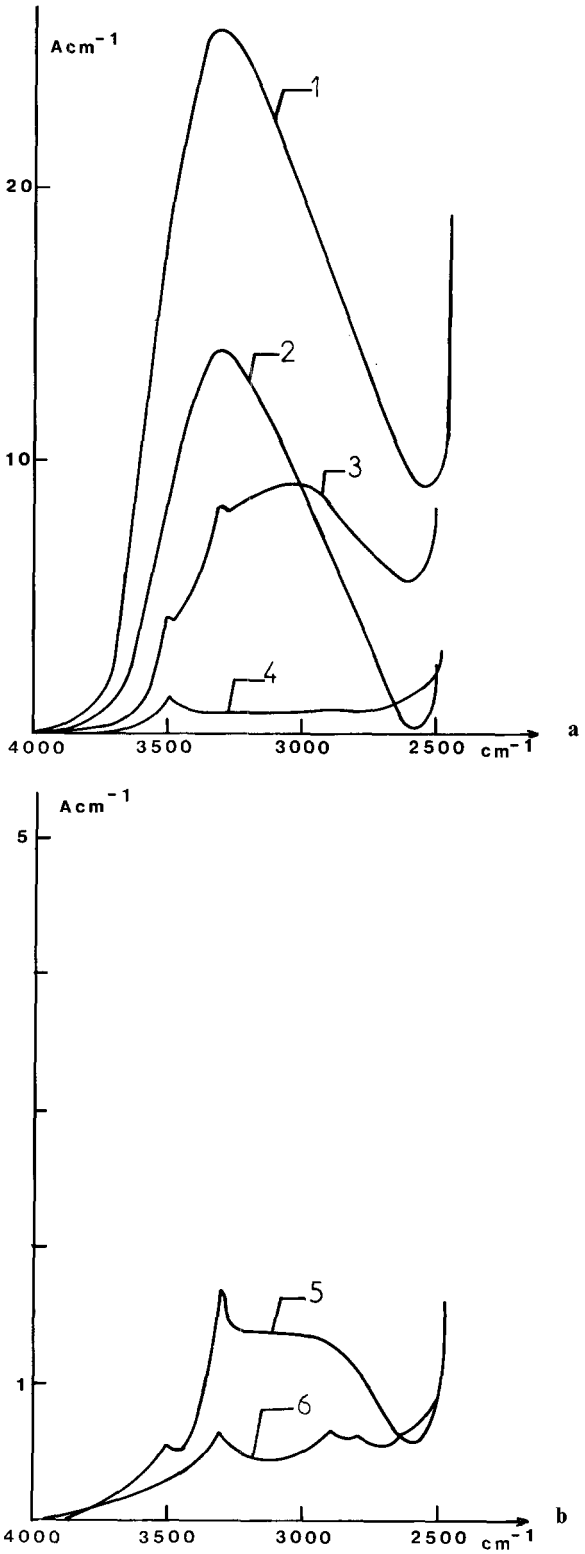

Fig. 1a, b. IR absorbance spectra of the as-grown berlinite crystals. Labels 1 to 6 refer to Table 1

of point defects. Griggs and Blacic who discovered the hydrolytic weakening phenomenon (Griggs and Blacic 1965; Griggs 1967, 1974) assumed that they were interstitial water molecules located in the **c** channels. Later on Nutall and Weil (1980) and Well (1984) have shown by *electron spin resonance* (ESR) that some substitutional defects noted

Table 1. Growth conditions and water content of some of the berlinite crystals used in this study

Sample number	Growth technique	Growth temperature	Filling of autoclave	Nutrient	Sample thickness	Water content	
						H_2O weight	H/Al+P at ppm
1	*HGM*	175° C	80%	H_3PO_4, 6*M*	200 μm	950 ppm	21000
2	*SHM*	150–190	–	–, 6*M*	190	650	10000
3	–	210–225	–	–, 8*M*	360	255	8500
4	–	225–245	–	–, 8*M*	510	83	1200
5	–	250–277	–	–, 10*M*	410	32.5	600
6	–	250–277	–	–, 12*M*	185	25	1000
7	*SHM, WIS*	180–200	–	–, 6*M*	very heterogeneous		
8	*SHM*	200–220	–	–, 8*M*			4000
9	–	230	–	acid solut.			–
10	–	–	–	–			–

HGM means Horizontal Gradient Method; *SHM* means Slow Heating Method (in this case the two values correspond to the starting and the finishing temperature respectively). *WIS* means Without Initial Seed. Samples 1 to 6 and 9 and 10 have been grown at the University of Montpellier (Laboratoire de Chimie des Matériaux). Sample 7 has been grown by GEC, Wembley UK and sample 8 by SICN, Annecy

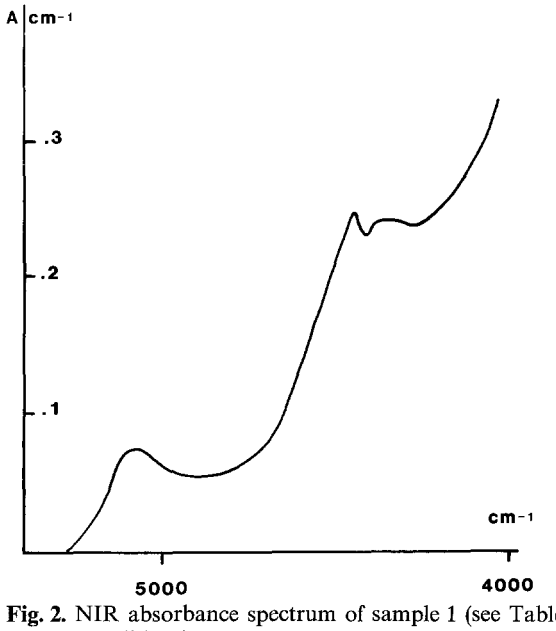

Fig. 2. NIR absorbance spectrum of sample 1 (see Table 1 for the growth conditions)

$(4H)_{Si}$ or $(2H_2O)_{SiO_2}$ also occur with a low concentration in high quality quartz. A somewhat similar defect has been detected by the same technique in berlinite by Halliburton et al. (1980). Recently Aines et al. (1984) have shown that water truly dissolved in quartz can be distinguished from tiny water inclusions by means of *near infrared* (NIR) spectroscopy in the range 7000–4000 cm^{-1}. Molecular water in the fluid inclusions induces an absorption peak in the vicinity of 5200 cm^{-1} (the corresponding vibration mode of the H_2O molecule is a combination of stretching and twisting of the OH bonds). In contrast the OH's stuck to Si atoms (the point defects) present an absorption peak in the vicinity of 4350 cm^{-1}. It seems that in most synthetic quartzes an important part of the water content occurs as tiny fluid inclusions but no quantitative relationship between peak height and water concentration of one or the other type has been calibrated yet. This new characterization technique has been applied to our berlinite crystals.

Fig. 2 shows the NIR absorbance spectrum of a very wet sample (number 1 of Table 1). An absorption peak is clearly visible at 5200 cm^{-1} and by analogy with the case of quartz, we attribute it to water inclusions. In the region 4400–4300 cm^{-1} two neighbouring absorption peaks may be observed attributable to water point defects of various types. We imagine the following types:

i) Interstitial water molecules. They should be able to occupy two distinct sites in the crystal structure in order to give rise to two distinct peaks.

ii) Substitutional water defects analogous to the $(4H)_{Si}$ defects of quartz. For instance they could be $(4H)_{Al}$ and $(3H)'_P$, the superscripts $^\cdot$ and $'$ meaning that they would be positively and negatively charged respectively. In the absence of any other impurities or point defects their concentrations should be equal (electrical equilibrium).

iii) Two H compensated antisites $(Al)_P$. Such antisites would result from a very slight non-stoichiometry in the molar ratio Al_2O_3/P_2O_5 but electric neutrality is preserved and no oxygen vacancy is formed if every P_2O_5 removed is replaced by one Al_2O_3 plus two H_2O leading to two $2H-(Al)_P$'s.

We have tested the influence of temperature and crystal orientation on NIR absorbance. The results are reported on Fig. 3. They show that temperature has practically no influence in the range tested 30–300 K. At low temperature the peaks become sharper and they are slightly shifted towards lower wave numbers but these changes are small. The crystallographic orientation mostly affects the background level attributed to the intrinsic absorption of the lattice. The peak to background ratio is maximum for an unpolarized beam propagating along the **c** direction. The NIR absorbance spectra of some other crystals of Table 1 are shown in Fig. 4. All have been recorded with basal samples. They show that the intensities of both peaks vary from sample to sample and this supports our hypothesis that these peaks are to be related to the two types of water in berlinite. Keeping in mind the total amount of water reported in Table 1, one sees that the water incorporated as the growth temperature is increased is related to the decrease of the peak at 5200 cm^{-1} attributed to water inclusions. We have verified that these fluid inclusions are mostly incorporated at the beginning of the growth process in char-

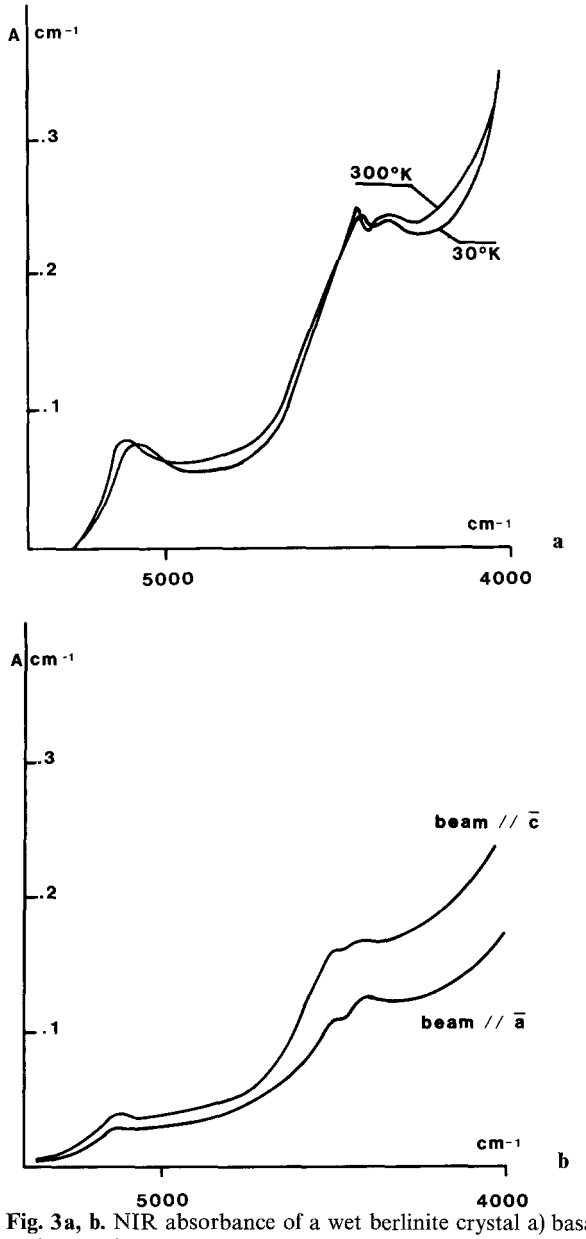

Fig. 3a, b. NIR absorbance of a wet berlinite crystal a) basal slab, variation of the spectrum with temperature b) influence of the crystallographic orientation at room temperature

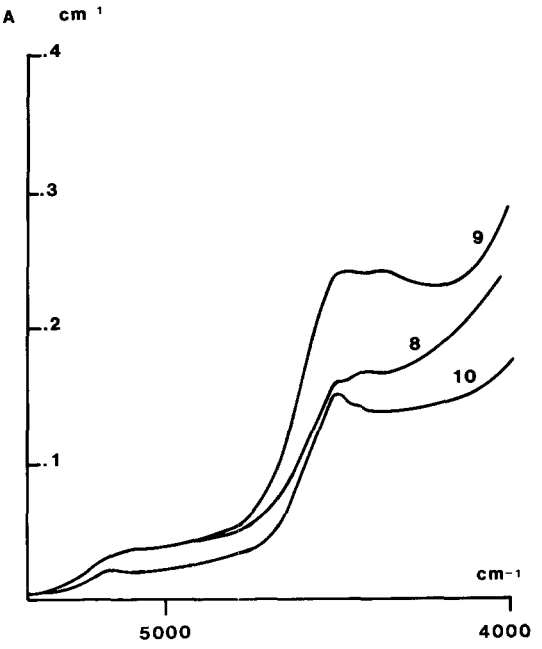

Fig. 4. NIR absorbance at 300 K of various crystals (labels according to Table 1)

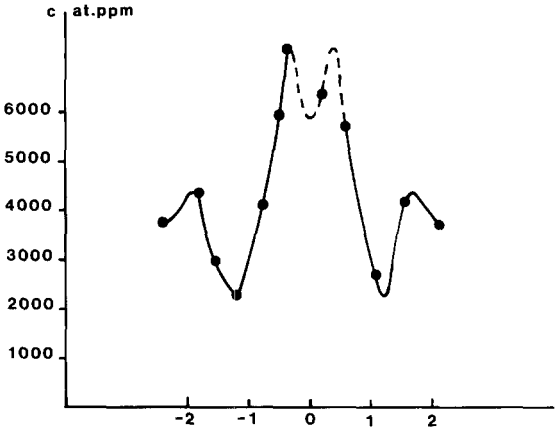

Fig. 5. Total water content profile along the growth direction **c** (content estimated with formula 2)

acterizing the concentration profile of water in a relatively dry crystal grown at elevated temperature and along the **c** direction. We have cut this crystal in thin and parallel slabs with a very thin diamond saw (150 μm) and we have measured the water content of each slab by conventional infrared spectroscopy (range 4000–2500 cm^{-1}). The resulting profile is shown in Fig. 5. As the intrinsic absorbance of dry berlinite is unknown, the zero of the vertical axis is not precisely known and only differences in concentrations are to be considered. Far from the seed, one observes on both sides a low concentration which might correspond to the true solubility of water in berlinite at the corresponding growth conditions. As one progressively moves towards the seed from either end the water content increases. The maximum increase $\Delta([H]/[Al+P]) \approx 5000$ at. ppm occurs in the immediate vicinity of the seed, then it falls down to a much lower value in the seed itself which comes from a dry crystal. The high water concentrations are thus related to high growth rates at the beginning of the process when the seeds are introduced into the nutrient (because of the reverse solubility one cannot heat the nutrient and the seeds together, these later ones would dissolve at low temperature). It has not been possible to confirm by NIR spectroscopy that the very wet regions do contain molecular water because this later technique requires samples one order of magnitude thicker than the ones for conventional IR spectroscopy (NIR absorbance is one order of magnitude lower than conventional IR absorbance).

We have also annealed a wet sample and recorded its new spectrum (Fig. 6) in order to estimate the evolution of the two distinct absorption peaks. It was expected that the peak associated to point defects would decrease while the one associated to water inclusions would increase. After annealing for 6 hours at a moderate temperature (315° C)

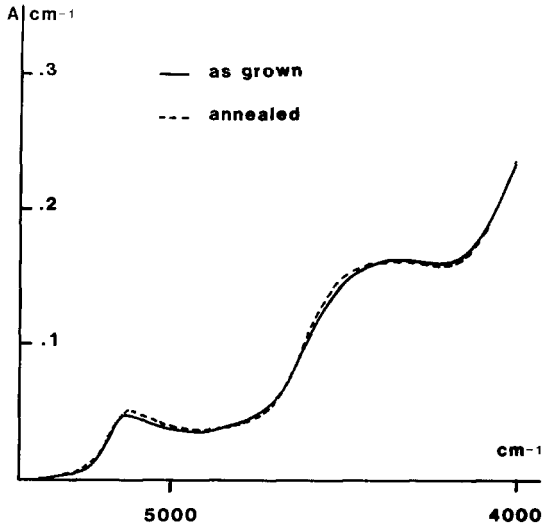

Fig. 6. Influence of annealing on the NIR spectrum: solid line = as-grown crystal; broken line = same crystal after 14 h annealing at 315° C

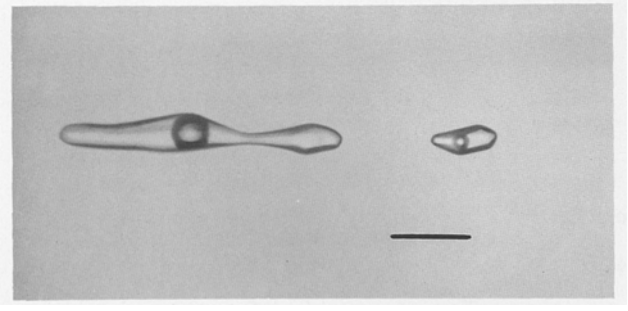

Fig. 7. Elongated inclusions near the seed (optical micrograph, scale bar = 20 μm)

a slight increase of the peak at 5200 cm^{-1} and a slight decrease of the two neighbouring peaks at 4400–4300 cm^{-1} are effectively detected. For longer anneals at higher temperatures the sample becomes milky. This later phenomenon obscurs the NIR spectra, preventing any calibration.

A number of *optical microscopy* (OM) and TEM investigations have been performed on as-grown samples with a view to detect the fluid inclusions incorporated during growth. OM observations are more easily performed with the samples being immersed in benzyl alcohol, a liquid with almost the same refractive index as berlinite. By this technique it has been possible to detect in some samples elongated fluid inclusions located mostly near and in the seeds (Fig. 7). Such holes in the seeds have probably been performed by preferential etching along the dislocations of the seeds when they were immersed in the nutrient. Like for the case of quartz, hollow tunnels decorating the dislocations would be formed by this process. Even if the temperature is correctly fitted to prevent seed dissolution or large growth rate, such an etching process can occur because the solubility of the atoms in the dislocation cores is larger than that at the seed surface. Except for these large inclusions no other defects are detected by OM. By TEM very tiny spherical holes (typical radius 50 to 100 Å, see Fig. 8) can be detected in the wettest crystals. They must correspond to the minute fluid inclusions incorporated during growth. Assuming that they were filled with liquid water

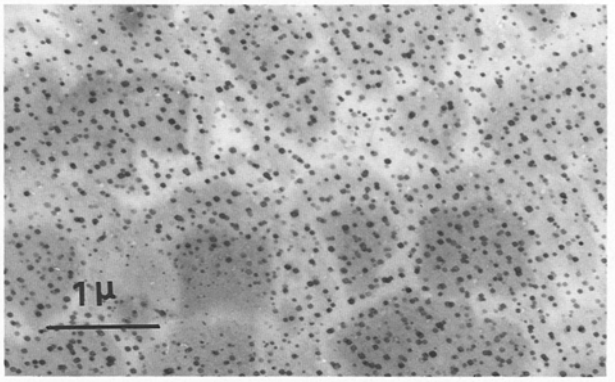

Fig. 8. Tiny fluid inclusions in a very wet as-grown crystal (n° 2 of Table 1)

during growth, a rough estimate of the density of inclusions $\approx 1.15 \times 10^{15}$ cm^{-3} leads to a water content [H]/[Al + P] ≈ 11000 at. ppm, in qualitative agreement with the results obtained by conventional IR absorption. It is possible that the sample contains further water inclusions so small that they could not be detected by TEM. This would not affect seriously the above estimate, however, because their contribution to the total water content varies as r^3 and would be negligible (r = inclusion radius). TEM investigations have also been performed after annealing at various conditions. As most of the water is already precipitated into small fluid inclusions the annealing process mostly affects the distribution of this precipitated water. Inclusion coalescence occurs, leading to larger precipitates which we call bubbles or water precipitates in the following. In most crystals we observed a large density of such water precipitates. These bubbles occur alone or are connected to small dislocation loops. This situation is very similar to the one already observed in wet synthetic quartz (McLaren et al. 1983). The disclocation loops which are sessile are nucleated to relax the fluid pressure in the bubbles. The mechanisms of water precipitation in wet quartz and wet berlinite have recently been investigated in detail (Doukhan et al. 1987, Cordier et al. 1988). These studies show that although most of the water was initially incorporated as molecular water (fluid inclusions) the evolution during annealing can only be interpreted to reflect point defect concentrations which are supersaturated. The results of NIR spectroscopy on wet berlinite are consistent with this point.

Extended Lattice Defects

The crystal structures of quartz and berlinite are identical; similar types of lattice defects are thus expected. However, two important differences have to be kept in mind:

i) The Si atoms of quartz are replaced in berlinite by Al and P with the sequence Al–P–Al–... along the **c** direction. As a consequence new extended defects can occur like antiphase boundaries (Van Tendeloo et al. 1976). Furthermore as **c** is twice larger, dislocations with **c** or **c**+**a** as Burgers vectors would have a line energy approximately four times larger. They are thus unlikely unless they dissociate. **c** dislocations may dissociate into two collinear partials 1/2 **c** + 1/2 **c** separated by a fault which happens to be the antiphase boundary mentioned above. For the **c**+**a** dislocations no simple dissociation model has been found.

ii) The Al–O and P–O bonds are weaker than Si–O

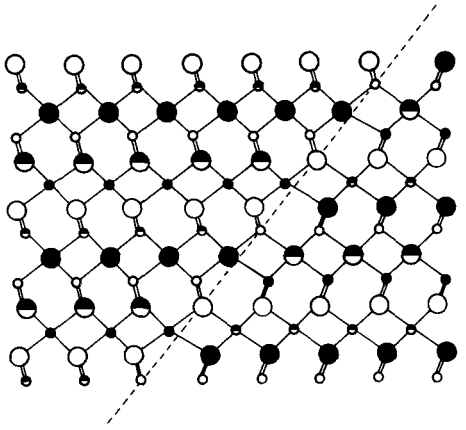

Fig. 9. Schematic representation of a Brazil twin with $(10\bar{1}2)$ as composition plane. The large circles represent the P atoms and the small circles the Al ones. The oxygen atoms are not represented but the Al—O—P bonds are symbolised by bars and the O atoms lie approximately in the middle of these bars

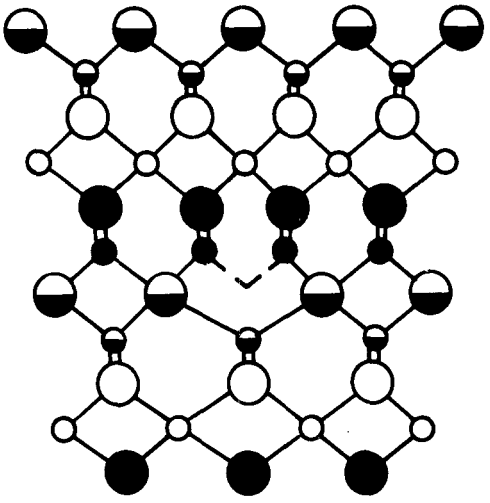

Fig. 10. Perfect **a** dislocation with a 60° character. The dislocation lies in the basal plane and is seen edge-on. Schematic representation with the same symbolism as in Figure 9. The reconstructed bonds are indicated by broken bars

bonds (Winkhaus 1951). As the glide mobility in these pseudocovalent structures is governed by the strength of the chemical bonds, marked differences in the elastic limits of dry crystals (without hydrolytic weakening effect) are expected. Furthermore Al—O bonds are weaker than P—O bonds; thus the easy glide systems of berlinite are those which break only Al—O bonds.

Twins

The two most frequent twins of α-quartz i.e. Dauphiné and Brazil twins have also been characterized in α-berlinite (Van Tendeloo et al. 1976, Doukhan et al. 1987). Dauphiné twin boundaries can occur on any surface in both minerals and vanish at temperatures above the $\alpha-\beta$ transition. Brazil twin boundaries can lie in (0001) and $\{10\bar{1}1\}$ planes in quartz. The later planes correspond to as-grown twins while the former ones are induced by deformation of dry quartz under very high stresses (McLaren et al. 1967). In both cases the twin boundaries are such that all the Si—O—Si bonds are reconstructed (i.e. every Si atom in the immediate vicinity of the twin boundary is at the center of a tetrahedron formed by four oxygen atoms and every tetrahedron shares its four corners with four adjacent tetrahedra owing to slight distortions of the Si—O—Si angles). In berlinite the situation is complicated by the fact that there are two kinds of tetrahedra AlO_4 and PO_4, each one sharing its corners with four tetrahedra of the other kind. Such a configuration has to be kept unchanged; otherwise antisites $(Al)_P$ and $(P)_{Al}$ would be nucleated and would increase the fault energy of the boundary. Clearly there is no such a problem with Dauphiné twinning in berlinite because the atomic relationships are not affected. For the case of Brazil twins a detailed examination of the structure (Fig. 9) shows that boundaries without antisites can be created in the (0001) and $\{10\bar{1}2\}$ planes. Until now only as-grown Brazil twins in the $\{10\bar{1}2\}$ planes have been observed.

Dislocations and Glide Systems

Figure 9 shows that there are two types of planes where dislocation glide only cuts the weaker Al—O bonds. They are the basal plane (0001) and the rhombohedral planes $\{10\bar{1}1\}$. The smallest lattice repeats in these planes are respectively the **a**'s $(1/3\langle 2\bar{1}\bar{1}0\rangle = 4.9\ \text{Å})$ in (0001) and $\mathbf{a}_2$ $(1/3[\bar{1}2\bar{1}0])$ and $\mathbf{c}+\mathbf{a}_3$ $(1/3[11\bar{2}3] \approx 12\ \text{Å})$ for the rhombohedral plane $(10\bar{1}1)$. Because $\mathbf{c}+\mathbf{a}$ would lead to a very large line energy for the corresponding dislocations, the expected easy glide systems are $(0001)1/3\langle 2\bar{1}\bar{1}0\rangle$ and $\{10\bar{1}1\}$ $1/3\langle 1\bar{2}10\rangle$. Furthermore, there are two possible levels for each glide plane such that only Al—O bonds are broken. For each glide system two distinct core structures have thus to be considered in strong analogy with the shuffle and glide sets of the covalent semi-conductors (for a recent review of these dislocation core properties, Heggie 1984). Fig. 10 is a schematic representation of a perfect $\mathbf{a}_2$ dislocation in the basal plane. It has a 60° character which is the preferred orientation left by deformation at low temperature controlled by Peierls friction. In this figure, the level of the glide plane in the unit cell has been chosen in such a way that there are two dangling bonds per lattice repeat along the $\mathbf{a}_3$ direction of the dislocation line. They lie on two adjacent Al atoms (in the other possible core configuration both dangling bonds would lie on the same atom; one passes from one configuration to the other by a climb motion of 1/6 **c**). We suggest that the glide plane of this dislocation is in fact a surface undulating between the O—Al layer and the Al—O one just beneath it. Such a situation presents two advantages: i) the dangling bonds are now equally distributed on the Al and O atoms and the dislocation core is rigourously neutral, even if the bonds were polarised and ii) the dislocation core can now be easily reconstructed owing to some moderate tilts and elongations of the dangling bonds. This reconstruction is very similar to the one already suggested for quartz (Doukhan and Trepied 1985, Heggie and Jones 1986). Such a core structure which minimizes the core energy is possible only for some directions such that the dangling bonds are near one another and have the right orientation for reconstruction. These are the preferred orientations parallel to the **a** directions in the basal plane which are observed after deformation at low temperature. In dry crystals or in conditions such that no hydrolytic weakening effect can occur (for instance at low temperature when the motion of water defects is hindered) the glide motion of these dislocations is controlled by the nucleation

and the propagation of double-kinks. A double-kink with a length $n\mathbf{a}$ requires breaking $2(n+1)$ Al−O bonds. The corresponding nucleation energy G_{kk} is thus approximately equal to $2(n+1)E_{\text{Al-O}}$ where $E_{\text{Al-O}}$ is the Gibbs energy necessary to break an Al−O bond in the dislocation core (one neglects the elastic energy of interaction of the two kinks). The minimum energy of nucleation of a double-kink thus corresponds to $n=1 (G_{kk} \approx 4E_{\text{Al-O}})$ and the corresponding double-kink has a minimum length equal to the unit lattice repeat a. Propagation of each elementary kink requires in turn breaking 2 Al−O bonds per elementary step of propagation. In deformation conditions such that no hydrolytic weakening occurs measurements of the elastic limit and of the density of mobile dislocations should thus allow the determination of this energy $E_{\text{Al-O}}$ necessary to break an Al−O bond in a dislocation core. We come back to this problem in the discussion.

Plastic Deformation

Deformation tests have been performed with a view to characterize the glide systems of berlinite and to test the possible role of water on the mobility of dislocations (hydrolytic weakening). Two types of tests have been performed:

i) Room temperature deformation in a Griggs machine (the confining pressure is necessary to prevent fracture). The aim of these tests was to characterize the intrinsic behaviour of dislocations in conditions such that no hydrolytic weakening phenomenon would occur (the water point defects are supposed to be immobile at room temperature and very few contacts between the mobile dislocations and the water inclusions are expected).

ii) Deformation at atmospheric pressure and at temperature below the α-β transition, at conditions for which the water point defects become mobile and the mobile dislocations can interact continuously with water (point defects as well as water inclusions). Hydrolytic weakening, whatever its exact microscopic mechanism, can thus occur.

1. Room Temperature Tests

We have used a viscous synthetic rubber as a confining medium in the Griggs machine. This provides good hydrostatic conditions (up to 1000 MPa) without appreciable deviatoric stresses. The recorded stress-strain curves for constant strain rate tests at room temperature are reported on Fig. 11. For comparison we also report the results for a quartz sample compressed at the same conditions. It exhibits a strictly elastic behaviour up to an ultimate deviatoric stress $\sigma_3 - \sigma_1 \approx 7000$ MPa at which it breaks explosively. In contrast, berlinite exhibits a ductile behaviour at reasonable flow stresses. Three different orientations have been tested. Orientation 1 at 45° to **a** and **c** (the so-called "O^+" orientation) promotes **a** basal glide. Orientation 2 at 45° to $\mathbf{a}_1$ and $\mathbf{a}_2$–$\mathbf{a}_3$ presents a large Schmid factor ($\phi = 0.45$) for the rhombohedral glide system $(01\bar{1}1)[2\bar{1}\bar{1}0]$ and a zero Schmid factor for basal **a** glide. Orientation 3 is parallel to **c** and has non vanishing Schmid factors only for **c**+**a** glides in rhombohedral planes. The observed macroscopic elastic limits are ≈ 500 MPa for the first orientation and 1500 MPa for the second orientation. In the third case no plastic deformation could be performed, the samples break explosively at deviatoric stresses >2000 MPa, a fracture strength markedly lower than that of quartz. This larger

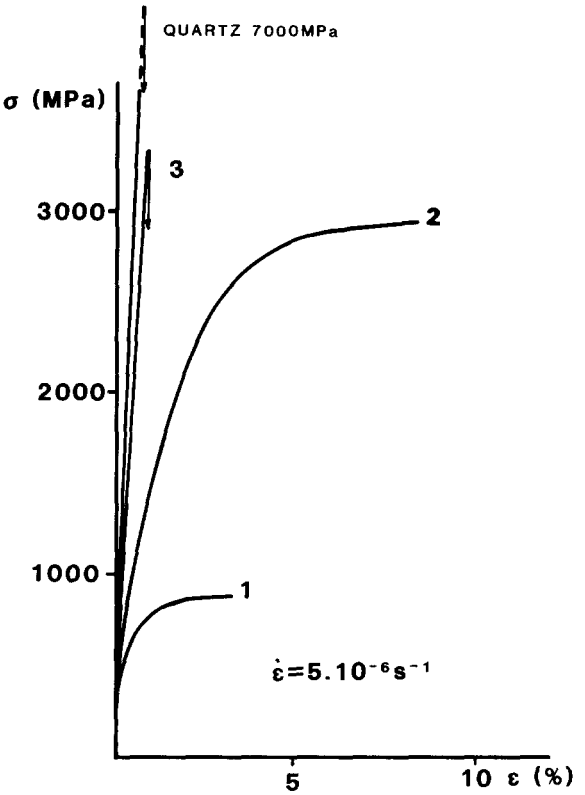

Fig. 11. Deformation at constant strain rate at room temperature and under a confining pressure $P = 600$ MPa. See text for the orientations corresponding to the labels 1 to 3

brittleness of berlinite could originate in the elongated fluid inclusions occurring in the vicinity of the seed (the actual size of synthetic crystals is small and samples with their large dimension parallel to **c** necessarily contain the seed).

The induced dislocation microstructures have been investigated by TEM. In samples with orientation 1 we observe, as expected, **a** dislocations in the basal plane. They exhibit a marked preferred orientation corresponding to a $\pm 60°$ character and they are homogeneously distributed after 1.5 percent plastic strain. Their density is $\approx 2 \times 10^{12}$ m^{-2} and does not change as the strain increases up to ≈ 5 percent. These results are consistent with a deformation regime controlled by a Peierls friction (Friedel 1967, Hirth and Lothe 1971). As the starting material has a rather low initial dislocation density (order 10^8 m^{-2}) a severe dislocation multiplication must occur at the beginning of the deformation process. Such a multiplication phenomenon generally induces a yield drop at the beginning of the stress-strain curve. No drop is observed in the present case. It has not been observed in the case of GaAs crystals deformed in similar conditions (Lefebvre et al. 1985) but it occurs in the case of silicon (Rabier et al. 1983). We do not know at the moment if this absence of yield drop is an artifact due to some friction in the Griggs machine or if the multiplication process is a very gradual one. Fig. 12 shows a typical dislocation configuration after 1.8 percent deformation.

In samples with orientation 2, we observe in the activated rhombohedral planes a dislocation density so high that the individual dislocations cannot be resolved. Furthermore there is abundant evidence of cross-slip of the **a** screw dislocations in the basal plane although the Schmid factor for basal **a** glide is zero. Cross-slip is thus probably due to

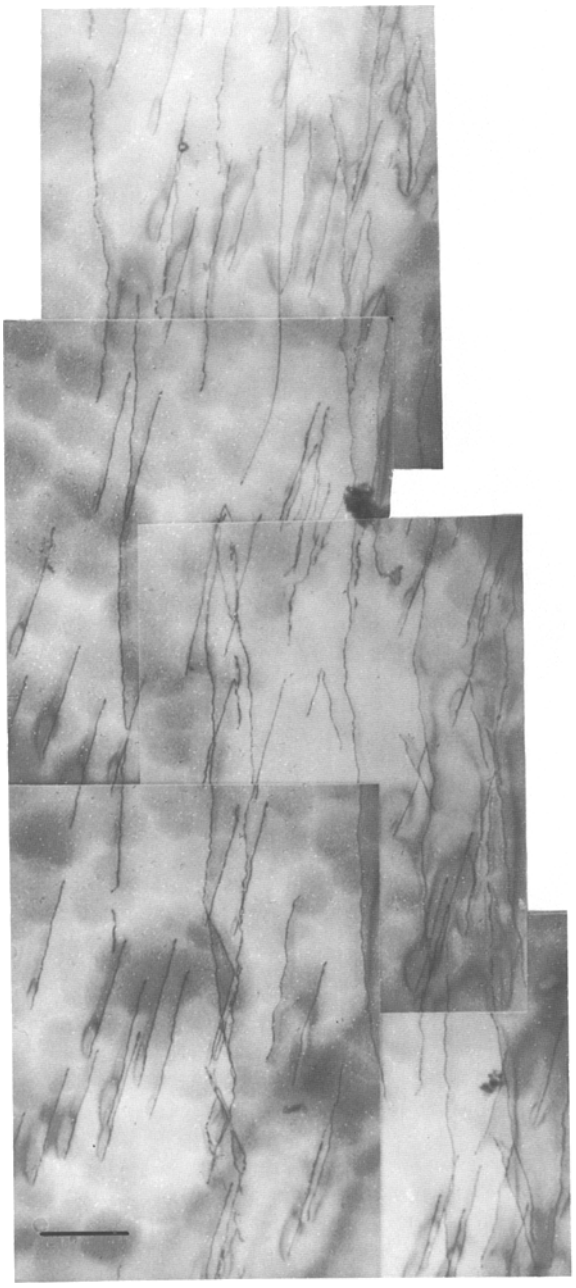

Fig. 12. Typical dislocation configuration in a sample with orientation 1 promoting **a** basal glide. T=room temperature; P=600 MPa; total plastic strain ε=1.8 percent; (0001) thin foil; $\mathbf{g}=10\bar{1}2$; scale bar=2 μm

the internal stresses. Numerous small cracks are also visible. As many dislocation lines are found to continue on both sides of the fracture edges, we presume that these fractures occurred under the action of large internal stresses when the confining pressure was progressively removed at the end of the experiment. Fig. 13 is a typical microstructure as observed in TEM. **a** glide in rhombohedral planes thus appears to be much less easy than in the basal plane.

Influence of Temperature and Water

Constant strain rate tests have been performed at atmospheric pressure in the temperature range 20–500° C using smaller samples (approximately $2\times2\times6$ mm^3). Even so it

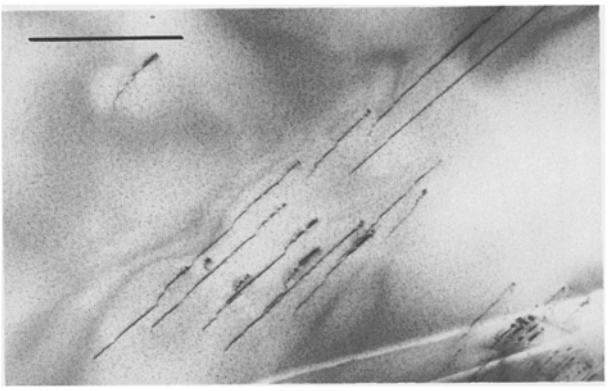

Fig. 13. Typical dislocation configuration in a sample with orientation 2 promoting rhombohedral **a** glide. T=room temperature; P=600 MPa; total plastic strain ε=5 percent; thin foil $(10\bar{1}0)$; $\mathbf{g}=01\bar{1}\bar{2}$; scale bar=1 μm

was not always possible to cut samples in regions which did not contain the seed. The same orientations have been tested. Below ≈250° C no plastic strain can be obtained, brittle fracture occurs for applied stresses of the order of 200 to 300 MPa even with the lowest cross-head speed of our Instron machine ($\dot{\varepsilon}\approx5\times10^{-6}$ s^{-1}). In TEM no special feature is detected in these samples which look identical to the as-grown material. Above 250° C, TEM investigations show that some water precipitation has occurred during the time necessary for a deformation test (typically a few hours). This clearly shows that plastic strain can be obtained under moderate stresses only when it is associated with water precipitation, i.e. when the water point defects become mobile. Water precipitation can generate a large density of small dislocation loops around the tiny precipitated bubbles. Such loops could then act as sources; water point defects can also diffuse towards the dislocation cores and facilitate kink and (or) jog nucleation along the dislocation lines, thus enhancing their glide (or climb) mobilities.

Some stress-strain curves are reported on Fig. 14. As can be seen the flow stress decreases as the temperature increases for both orientations. Above 300° C yielding is followed by work-hardening with a hardening rate which increases with increasing temperature. As for wet quartz, this phenomenon is associated with water precipitation which accompanies the deformation. The activation volume has been measured all along the deformation curves by the stress relaxation technique (Dotsenko 1979). This volume decreases rapidly as the deformation proceeds, then it stabilises at very low values of the order of 300 Å^3 for $\varepsilon\approx1$ to 2 percent. All these facts are consistent with a thermally activated deformation regime. However the dislocation microstructures of the deformed samples differ from those expected for such a regime, in which dislocations are well confined within their glide planes and marked preferred orientations develop. In contrast we observe a large density of bubbles with various sizes and dislocation segments connected to them. These dislocations are not confined within the expected glide planes (0001) or $(10\bar{1}1)$. Many dislocation junctions are also observed which confirm that climb processes occurred at these moderate temperatures ($\leq1/3\,T_M$ where T_M is the melting temperature in K). Thus, these TEM observations provide information mostly on water precipitation and fluid inclusion coalescence, which obscure the dislocation substructure resulting from the deformation

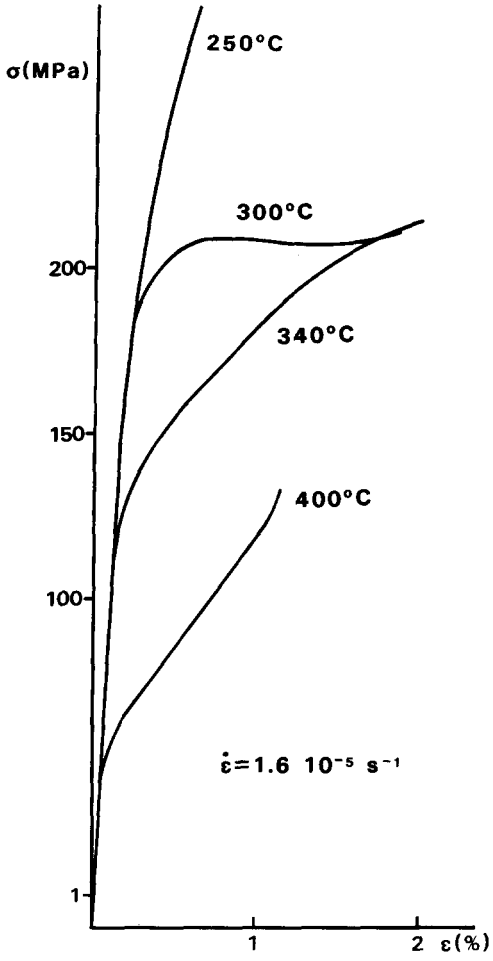

Fig. 14. Constant strain rate tests at atmospheric pressure. Orientation 2. The temperature of the test is indicated on each curve

process. A similar situation has already been described in the case of wet quartz (Doukhan and Trepied 1985) but it becomes pervasive only for large deformations (or longer deformation times). It seems that in berlinite, because of its large water content, the onset of this process occurs at lower strains (2%). It is also possible, however, that the dislocation configuration changes during the slow cooling stage which follows the deformation itself. Bubbles would thus continue growing at relatively low temperature and as a result the dislocations would reach a climb configuration in absorbing the atoms removed from the bubble surfaces. As a consequence it is very difficult to obtain unambiguous information on the glide systems activated. Furthermore there is another unexpected observation which may be noted. In samples with orientation 2 deformed at or above 300° C, we observe **c**+**a** dislocations with a density of the order of 10^{12} m^{-2} (this density apparently increases with the total plastic strain i.e. with the duration of the test). The dislocations are most often found in junctions with a Burgers vector reaction $(\mathbf{c}+\mathbf{a}_3)+\mathbf{a}_2 \rightarrow (\mathbf{c}-\mathbf{a}_1)$ (see Fig. 15). No free **c**+**a** dislocations (i.e. not belonging to a junction or not connected to a bubble) or **c** dislocations are found. The Schmid factor for the most favoured **c**+**a** glide (in a rhombohedral plane) is only 0.27. No ductile behaviour could be obtained however with the samples with orientation 3 which should promote **c**+**a** glide only. No **c**+**a** dislocations are found in samples with orientation 1

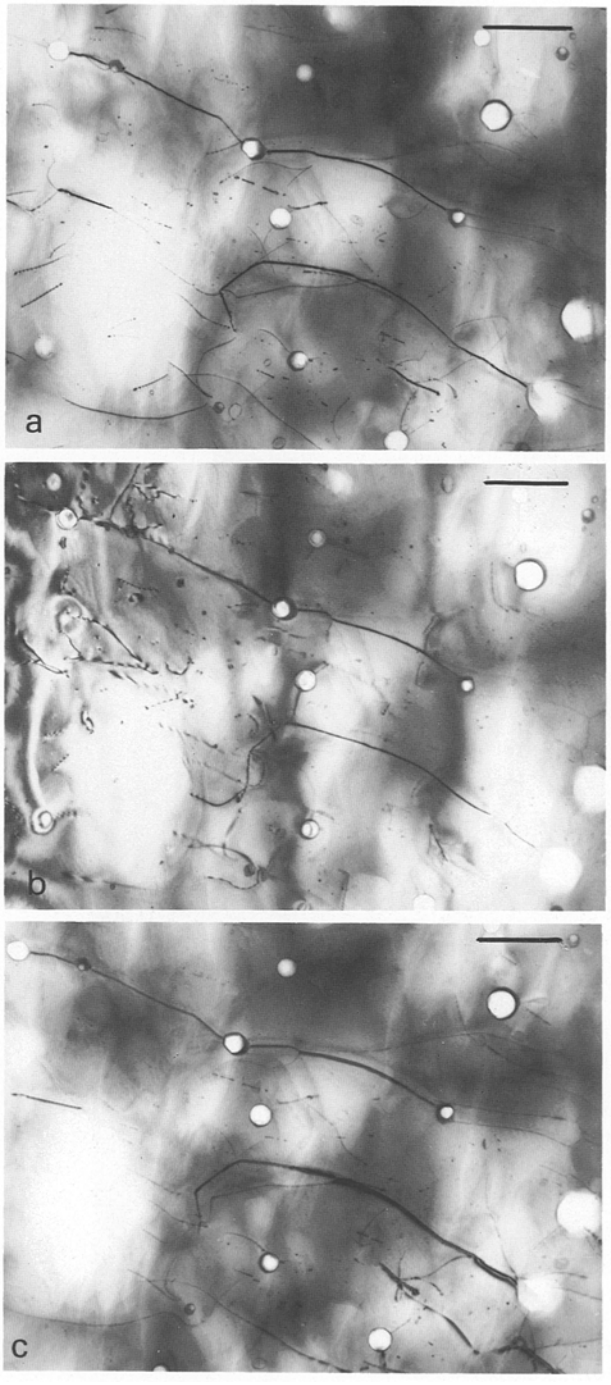

Fig. 15a–c. **c**+**a** dislocations in a junction. Sample deformed at T=500° C. Orientation 1; thin foil perpendicular to the deformation axis; scale bar = 1 μm (**a**) $\mathbf{g}=01\bar{1}\bar{2}$ (**b**) $\mathbf{g}=1\bar{1}0\bar{2}$ (**c**) $\mathbf{g}=10\bar{1}\bar{2}$

although the most favoured **c**+**a** glide system has a Schmid factor very similar to the one computed for orientation 2. We therefore suggest that these **c**+**a** dislocations are related to water precipitation rather than to the plastic deformation process itself. Sessile **c**+**a** dislocation loops could have been nucleated at the contact of the bubbles to relax their pressure. Previous TEM investigations on annealed samples revealed loops with Burgers vectors **a** and not **c**+**a**. We can thus suppose that the applied stress provides a work contributing to the energy required to nucleate a sessile **c**+**a** loop. This contribution may be larger for the orientation

2 owing to geometric factors analogous to the Schmid factor (but for a climb configuration). Such an energy is at most $\approx\sigma(\mathbf{c}+\mathbf{a})^3$. Considering the maximum flow stress, this energy cannot exceed 0.5 eV which is a very low value for the nucleation energy of a sessile dislocation loop with such a large Burgers vector; thus, the origin of these **c**+**a** dislocations remains unelucidated at the moment.

Discussion, Comparison with Quartz

There are numerous similarities and some marked differences between quartz and berlinite. Both crystals have the same structure but **c** is twice as long and the bond strengths are weaker in berlinite (especially the Al−O ones). Both are grown in aqueous solutions and can contain water which results in a reduction in strength. The mechanisms of this weakening effect seem to be essentially the same in both cases and we distinguish two possible phenomena:

i) Mobile water point defects diffuse towards the dislocation cores and facilitate the nucleation of kinks and/or jogs, thus allowing an enhanced glide and/or climb dislocation mobility.

ii) At the contact of a mobile dislocation with a fixed fluid inclusion or a bubble a single kink or a jog is easily nucleated and propagates along the dislocation line (this later process beeing thermally activated).

The intrinsic behaviour of dislocations in berlinite is probably evaluated best by the experiments performed at room temperature under confining pressure although the crystals are not dry. Indeed, for the above conditions, water defects are immobile and there are very few contacts along the dislocation lines where they could assist the nucleation of a kink or a jog. If the crystals are not too wet we can also assume that the density of contacts with fluid inclusions or bubbles is also relatively low. We thus assume that the observed Peierls regime is controlled by the thermally activated nucleation of elementary double-kinks one unit repeat long (this is the value indicated by the stress relaxation experiments performed at $T\approx 400°$ C). For basal **a** glide the formation of an elementary double-kink requires breaking 4 Al−O bonds. Let E be the energy of such a bond in the dislocation core. For **a** basal glide this nucleation corresponds to an area swept by the dislocation $S=3a^2\sqrt{3/2}$; the work done by the reduced stress $\tau=\sigma$. ϕ is equal to $\tau . S . a$ The thermal equilibrium concentration of elementary double-kinks (intrinsic concentration) along such a dislocation line is thus:

$$c_{kk}(T,\tau)=\exp-\frac{4E-3\sqrt{3}\,\tau a^3/2}{kT}. \tag{3}$$

For an **a** dislocation with a 60° character, the two kinks are not equivalent. One has a screw character while the other has a 120° one. As we have not observed screw dislocation segments among the dislocations left by the deformation, we assume that the screw segments, as well as the screw kinks, have a relatively large mobility. The other kink when it moves has to break two Al−O bonds per elementary step. Its velocity is thus:

$$v_k=\nu a\exp-\frac{2E-\tau a^3\sqrt{3}}{kT} \tag{4}$$

where ν is the Debye frequency. Let $d=a/c_{kk}$ be the mean distance between adjacent elementary double-kinks. As the screw kinks are assumed to have a larger mobility than the 120° ones, we assume in a somewhat arbitrary manner that they move over $3d/4$ while the 120° kinks only move over $d/4$. The resulting dislocation mobility is $v_d=4c_{kk}v_k$. The Orowan equation can thus be written

$$\dot{\gamma}=\rho a v_d=4\nu a^2\rho\exp-\frac{6E-5\tau a^3\sqrt{3}/2}{kT} \tag{5}$$

$\dot{\gamma}$ is the reduced strain rate. The experiments provide the following data: $\dot{\gamma}=10^{-5}\,s^{-1}$; $\rho=2\times10^{12}\,m^{-2}$; $\tau=500$ MPa. We assume that ν, the Debye frequency, is $10^{13}\,s^{-1}$; this leads to a value of the Gibbs energy necessary to break an Al−O bond in the dislocation core $E=0.25$ eV. In dry quartz Doukhan and Trepied (1985) have estimated the corresponding energy for a Si−O bond of the order of 2 eV. This therefore accounts for the much lower strength of berlinite at room temperature. A similar calculation can be made for the case of rhombohedral **a** glide. A detailed examination of the structure indicates that the nucleation of an elementary double-kink along an edge dislocation requires breaking 8 Al−O bonds. Both single kinks are identical in this case and have a screw character; their propagation does not require any further breaking of Al−O bonds. Numerical data for this system are: $\dot{\gamma}=10^{-5}\,s^{-1}$; $\rho=2\times10^{16}\,m^{-2}$; $\tau=1500$ MPa. They lead to a very similar value for E. This model of dislocation glide mobility controlled by the breaking of the pseudocovalent bonds thus appears to be consistent.

In fact the experiments performed at room temperature are not perfectly identical to tests on dry crystals. Indeed, the tiny inclusions play a hardening effect in pinning the mobile dislocations. Let d be the diameter of a spheric inclusion. A dislocation line connected to such an inclusion decreases its line energy by an amount $\approx d\times\mu b^2/2$ (b=Burgers vector modulus; μ=shear modulus). This corresponds to a pinning force which is roughly proportional to d i.e. large bubbles must lead to scallopped configurations like that shown on Fig. 16. However our experiments show that even for the wettest crystals tested this dragging force never exceeds the lattice friction related to the breaking of the Al−O bonds. A similar pinning effect by bubbles has been proposed by Kirby and McCormick (1979) for wet quartz.

As far as hydrolytic weakening would result in enhancing the *glide* mobility of dislocations only, it could simply consist in reducing the nucleation energy and the propagation energy of the double-kinks. However experiments show that a considerable amount of dislocation climb occurs in wet samples deformed at moderate temperatures ($T<T_M/3$) for which no climb would be expected in dry specimens. It is thus clear that water also enhances dislocation climb. As noted in the first section water enters in berlinite under two distinct forms, water point defects and tiny fluid inclusions. One or the other form, or both, enhance the glide and/or the climb mobilities of the dislocations. In the absence of further experiments on drier berlinite crystals, it is impossible to separate the role of point defects from the one of fluid inclusions. However recent experiments on quartz (Cordier and Doukhan 1989) show that in this later mineral, when water occurs essentially under the form of point defects with a concentration not larger than to the

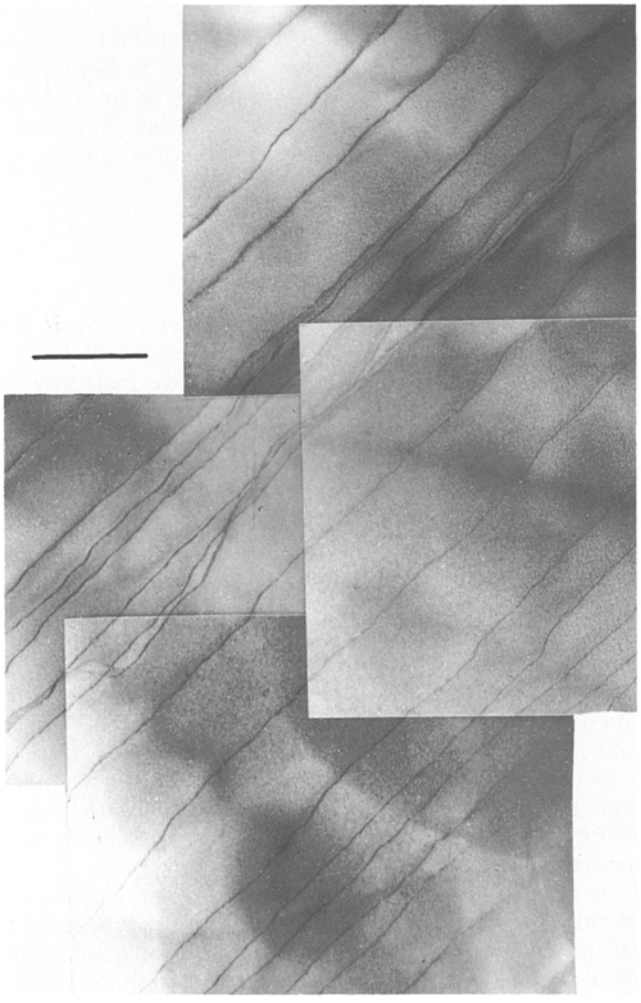

Fig. 16. Dislocations pinned on tiny fluid inclusions. Sample with orientation 1 deformed at T = room temperature; $P = 600$ MPa. The dislocations show a gross preferred orientation corresponding to a 60° character. They also present scallops with a slight curvature because of pinning. Scale bar = 2 μm

equilibrium one, the glide mobility of the dislocations is enhanced, but no climb effect is observed. In contrast for a concentration even slightly larger than the equilibrium one, and almost no fluid inclusions, climb becomes the prominent effect. This change from enhanced glide to enhanced climb is very sensitive to slight changes of the concentration of point defects. For instance, in the cited experiments, for a concentration of point defects H/Si $\approx$ 100 at. ppm corresponding to the equilibrium solubility at the conditions of deformation $T = 700°$ C and $P = 1000$ MPa, only glide is observed after ≈ 2 percent strain and the dislocations exhibit marked crystallographic orientations. In contrast for H/Si $\approx$ 180 at. ppm, and for the same T, P and ε conditions, subgrain-boundaries are observed after only 3 percent strain, which indicates that climb is pervasive. Water point defects have also precipitated in numerous tiny bubbles often connected to dislocations.

Several models have been proposed to interpret the hydrolytic weakening phenomenon in wet quartz. The first one elaborated by Griggs (1967, 1974) was based on the assumption that water is dissolved as interstitial molecules which would hydrolyse the strong Si−O bonds thus allowing an easier *glide* motion of the dislocations. McLaren and Retchford (1969) have proposed another model where it is rather the *climb* motion of the mobile dislocations which would be assisted by the water defects (point defects or tiny fluid inclusions). Both models can be considered as localised models i.e. the water defects – water molecules or OH hydroxyls – are active only when they are in contact with a dislocation line; they can thus assist the nucleation of a double-kink or a jog. More recently Hirsch (1981) and Hobbs (1985) have independently proposed non localised models which consider only point defects. These later ones would act like doping impurities in semi conductors; they would generate deep levels in the gap which in turn would generate a larger density of kinks and/or jogs. It is to be mentioned that the aim of all these models is to interpret the experimental results obtained with wet samples most always deformed in T and P conditions such that the state of dispersion of water continuously changes during a deformation experiment. This later parameter is never taken into account in the above models which are supposed to describe a steady-state regime while it is clear now that a steady-state is never reached as long as one does not use crystals with a concentration of water point defects $\leq$ the equilibrium one at the T and P conditions of deformation. Our most recent experiments suggest that under these conditions water point defects only assist dislocation glide. We suggest that a similar situation would occur in berlinite if crystals with a moderate concentration of point defects and almost no fluid inclusions were available and could be tested in a Griggs apparatus. At the moment only the situation corresponding to a large concentration of minute fluid inclusions has been tested. The experiments reported here correspond to a continuous evolution of the state of dispersion of the water content and no steady-state can be reached. These experiments do not allow a convenient interpretation of the role of water (hydrolytic weakening) in berlinite crystals deformed in a steady state. They rather reflect the evolution of bubble coalescence governed by bulk diffusion of water point defects. This phenomenon drives the diffusion of the Al, P and O atoms from the bubble surfaces (sources) to the dislocation cores (sinks). Marked climb dislocations structures thus result, even at moderate temperature. Such a phenomenon lates as long as there are several interacting bubbles i.e. which are not too far apart.

Acknowledgements. The authors thank CNET for financial support. They also acknowledge Dr. Philippot (USTL, Montpellier), Dr. Buisson (SICN, Annecy) and Dr. Todd (GEC, Wembley) for providing the crystals which have been studied here. The authors also thank Dr. Vignaud (Lille) who has kindly performed the NIR spectra on the various berlinite crystals.

References

Aines RD, Kirby SH, Rossman GR (1984) Hydrogen speciation in synthetic quartz. Phys Chem Minerals 11:204–212

Aines RD, Rossman GR (1984) Water in minerals? A peak in the infrared. J Geophys Res 84:4059–4071

Beran A (1986) A model of water allocation in alkali feldspars derived from infrared spectroscopy investigations. Phys Chem Minerals 13:306–310

Boland JD, Tullis TE (1986) Deformation behaviour of wet and dry clinopyroxenite in the brittle to ductile transition region. In: Hobbs BE and Heard HC (eds) Mineral and rock deformation (Geophys Monograph N° 36) Am Geophys Union, Washington, pp 35–49

Chai BHT, Hou JP (1987) Evaluation of berlinite grown at high temperature. Oral communication at First European Frequency and Time Forum, Besançon

Cordier P, Boulogne B, Doukhan JC (1988) Water precipitation and diffusion in wet quartz and wet berlinite. Bull Mineral 111:113–137

Cordier P, Doukhan JC (1989) Water in quartz; solubility and influence on ductility. Submitted to European J Mineralogy

Detaint J, Philippot E, Jumas JC, Schwartzel J, Zarka A, Capelle B, Doukhan JC (1985) Crystal growth, physical characterization and BAW device applications of berlinite. 39th Ann Freq Control Symp, pp 234–246

Dodd DM, Fraser DB (1965) The 3000–3900 cm^{-1} absorption bands and anelasticity in crystalline α quartz. J Phys Chem Solids 26:673–686

Dotsenko VI (1979) Stress relaxation in crystals. Phys Status Solidi (b) 93:11–43

Doukhan JC, Boulogne B, Cordier P, Philippot E, Jumas JC, Toudic Y (1987) A transmission electron microscope study of lattice defects and water precipitation in α berlinite. J Cryst Growth 84:167–179

Doukhan JC, Trepied L (1985) Plastic deformation of quartz single crystals. Bull Mineral 108:97–123

Freund F, Oberheuser G (1986) Water dissolved in olivine; a single crystal infrared study. J Geophys Res 91:745–761

Friedel J (1967) Dislocations. Pergamon Press, New York

Griggs DT (1967) Hydrolytic weakening of quartz and other silicates. Geophys J R Astron 14:19–31

Griggs DT (1974) A model of hydrolytic weakening in quartz. J Geophys Res 79:1653–1661

Griggs DT, Blacic JN (1965) Quartz, anomalous weakness of synthetic crystals. Science 147:292–295

Halliburton LE, Kappers LA, Armington AF, Larkin J (1980) Radiation effects in synthetic berlinite ($AlPO_4$). J Appl Phys 51:2193–2198

Halliburton LE, Martin JJ (1985) Properties of piezoelectric materials. In Gerber EA, Ballato A (eds) Acoustic resonators and filters. Vol I, Academic Press, New York, pp 1–45

Hirth J, Lothe J (1971) Theory of dislocations. McGraw Hill, New York

Hirsch PB (1981) Plastic deformation and electronic mechanisms in semi conductors and insulators. J Physique C3:149–160

Heggie MI (1984) The structure of dislocations, principally in silicon, inferred from experimental and theoretical results. In: Veyssiere P, Kubin L, Castaing J (eds) Dislocations 1984. Editions du CNRS, Paris, pp 305–314

Heggie MI, Jones R (1986) Models of hydrolytic weakening in quartz. Philos Mag 53:L65–L70

Hobbs BE (1985) The hydrolytic weakening effect in quartz. In: Schock (ed) Point defects in minerals (Monograph n° 31) Amer Geophys Union, Washington, pp 151–170

Jumas JC, Goiffon A, Capelle B, Zarka A, Doukhan JC, Schwartzel J, Detaint J, Philippot E (1987) Crystal growth of berlinite $AlPO_4$. Physical characterization and comparison with quartz. J Cryst Growth 80:133–148

Kats A (1962) Hydrogen in α quartz. Philips Res Reports 17:133–279

Kats A, Haven Y (1960) Infrared absorption bands in α quartz in the 3 μm region. Phys Chem Glasses 1:99–102

Kirby SH, McCormick JW (1979) Creep of hydrolytically weakened synthetic quartz crystals oriented to promote $\{2\bar{1}\bar{1}0\}\langle 0001\rangle$ slip. A brief summary of work to date. Bull Mineral 102:124–137

Kolb ED, Laudise RA (1978) Hydrothermal synthesis of aluminium orthophosphate. J Cryst Growth 43:313–319

Lefebvre A, François P, Di Persio J (1985) Transmission electron microscopy of semi insulating GaAs deformed at room temperature and under confining pressure. J Phys Lettres 46:L1023–L1030

Lipson HG, Kahane A (1984) Distribution of aluminium and hydroxide defect centers in irradiated quartz. 38th Proc Ann Freq Control Symp, pp 10–15

Lipson HG, Kahane A (1985) Infrared characterization of aluminium and hydrogen defect centers in irradiated quartz. J Appl Phys 58(2):963–970

McLaren AC, Retchford JA (1969) TEM study of the dislocations in plastically deformed synthetic quartz. Phys Status Solidi (1969) 33:657–668

McLaren AC, Retchford JA, Griggs DT, Christie JM (1967) TEM study of Brazil twins and dislocations experimentally produced in natural quartz. Phys Status Solidi 19:631–644

McLaren AC, Cook RF, Hyde ST, Tobin RC (1983) The mechanisms of formation and growth of water bubbles and associated loops in synthetic quartz. Phys Chem Minerals 9:79–94

Nutall RHD, Weil JA (1980) Two hydrogenic trapped hole species in α quartz. Solid State Commun 33:99–102

Palache C, Berman H, Frondel C (1970) The Dana's system of mineralogy. Vol II, Wiley, New York

Paterson MS (1982) The determination of hydroxyl by infrared absorption in quartz, silicate glasses and similar materials. Bull Mineral 105:20–29

Rabier J, Veyssiere P, Demenet JL (1983) Plastic deformation of silicon at low temperature and the influence of doping. J Physique C4:243–253

Stanley JM (1954) Hydrothermal synthesis of large aluminium phosphate crystals. Ind Eng Chem 46:1684–1689

Steinberg RF, Roy MD, Estes AK, Chai BHT, Morris RC (1984) Propagation loss characteristics of berlinite. IEEE Symp Ultrasonics 279–284

Van Tendeloo G, Van Landuyt J, Amelinckx S (1976) The α-β transition in quartz and $AlPO_4$ as studied by electron microscopy and diffraction. Phys Status Solidi(a) 33:723–735

Weil JA (1984) A review of electron spin spectroscopy and its application to the study of paramagnetic defects in crystalline quartz. Phys Chem Minerals 10:149–165

Winkhaus B (1951) Die Kristallchemischen Beziehungen zwischen Aluminium Orthophosphat $AlPO_4$ und Siliciumdioxyd SiO_2. Neues Jahrb Mineral Abh 83:1–22

Wood DL (1960) Infrared absorption of defects in quartz. J Phys Chem Solids 13:326–336

Received February 4, 1988